Nuclear Medicine and Biology 104–105 (2022) 38–46

Contents lists available at ScienceDirect

Nuclear Medicine and Biology

journal homepage: www.elsevier.com/locate/nucmedbio

Target manufacturing by Spark Plasma Sintering for efficient ^{89}Zr production

S. Cisternino [a,b,*], E. Cazzola [c,**], H. Skliarova [a,1], J. Amico [c], M. Malachini [c], G. Gorgoni [c], U. Anselmi-Tamburini [d], J. Esposito [a]

[a] Istituto Nazionale di Fisica Nucleare, Laboratori Nazionali di Legnaro (PD), Italy
[b] Dipartimento di Ingegneria Industriale, Università di Padova, Padova, PD, Italy
[c] IRCCS Ospedale Sacro-Cuore Don Calabria, Negrar di Valpolicella, VR, Italy
[d] Dipartimento di Chimica, Università di Pavia, Pavia, PV, Italy

ARTICLE INFO

Article history:
Received 30 June 2021
Received in revised form 10 November 2021
Accepted 22 November 2021

Keywords:
Zirconium-89
Spark plasma sintering
Cyclotron
Solid target
Radionuclide production

ABSTRACT

Zirconium-89 (^{89}Zr) is an emerging radionuclide for positron emission tomography (PET), with nuclear properties suitable for imaging slow biological processes in cellular targets. The ^{89}Y(p,n)^{89}Zr nuclear reaction is commonly exploited as the main production route with medical cyclotrons accelerating low-energy (< 20 MeV) and low-current (< 100 μA) proton beams. Usually, natural yttrium solid targets manufactured by different methods, including yttrium electrodeposition, yttrium sputtering, compressed yttrium powders, and foils, were employed. In this study, the Spark Plasma Sintering (SPS) technique has been investigated, for the first time, to manufacture yttrium solid targets for an efficient ^{89}Zr radionuclide yield. The natural yttrium disc was bonded to a niobium backing plate using a commercial SPS apparatus and a prototype machine assembled at the University of Pavia. The resulting targets were irradiated in a TR19 cyclotron with a 12 MeV proton beam at 50 μA. A dedicated dissolution module, obtained from a commercial system, was used to develop an automated process for the purification and recovery of the produced ^{89}Zr radionuclide. The production yield and recovery efficiency were measured and compared to ^{89}Zr produced by irradiating standard yttrium foils. SPS manufactured targets withstand an average heat power density of approximately 650 W·cm^{-2} for continuous irradiation up to 5 h without visible damage. A saturation yield of 14.12 ± 0.38 MBq/μAh was measured. The results showed that the obtained ^{89}Zr production yield and quality were comparable to similar data obtained using standard yttrium foil targets. In conclusion, the present work demonstrates that the SPS technique might be a suitable technical manufacturing solution aimed at high-yield ^{89}Zr radioisotope production.

1. Introduction

^{89}Zr radioisotope is considered a promising candidate for monoclonal antibody (mAb)-based positron emission tomography (immuno-PET) imaging due to its main features: (a) the physical half-life of 3.27 d compatible with the biodistribution time required for a mAb to achieve optimal tumor to non-tumor ratios; (b) the relatively low positron energy (maximum β^+ energy = 0.897 MeV, β^+ = 22.7%) suitable for high-resolution PET images; (c) straightforward production using a medium- to small-size medical cyclotron [1–3]. The nuclear reaction ^{89}Y(p,n)^{89}Zr, carried out irradiating a target composed of 100% naturally abundant Yttrium-89 material (^{89}Y or Y), is the most common route aimed at ^{89}Zr production. According to cross-section evaluation, the optimal proton energy to achieve the highest possible ^{89}Zr radionuclide yield while limiting radioisotopic contaminants production is in the range of 5–15 MeV, ideal for low-energy (i.e., medical) cyclotrons [3–5].

The interest in ^{89}Zr radioisotope for research purposes has grown in recent years, as confirmed by the Coordinated Research Project of the International Atomic Energy Agency (IAEA) [6] started in 2020. In this scenario, different groups worldwide have been working to improve the ^{89}Zr production steps, from target design and manufacturing, up to purification, recovery and labeling studies [2,3,5,7–12].

The choice of the proper target type plays a crucial role in the production of the radioisotope of interest. In view of a massive yield of radioisotopes, allowing their distribution and availability in different centers for conducting pre-clinical and clinical research trials, the use

* Correspondence to: S. Cisternino, INFN-LNL, Viale dell'Università, 2, Legnaro, PD, Italy.
** Correspondence to: E. Cazzola, Via Don A. Sempreboni 5, Negrar di Valpolicella, VR, Italy.
E-mail addresses: sara.cisternino@lnl.infn.it (S. Cisternino), emiliano.cazzola@sacrocuore.it (E. Cazzola).
[1] Present address: Belgian Nuclear Research Center (SCK CEN), Mol, Belgium.

https://doi.org/10.1016/j.nucmedbio.2021.11.004

of solid targets is considered the most prevalent choice [13]. As an alternative, the use of liquid target, in terms of target processing and cost, could be an option in the case where the medical cyclotrons do not include a solid target station. However, the ^{89}Zr yield thus obtained is significantly lower than the solid target case [14]. Furthermore, the radiolysis problem in the yttrium nitrate solution is an open issue investigated in several studies [15–17].

In our previous work, we have already reported a comparison study between the most common solid target preparation methods [18], such as electrodeposition, sputtering, compressed powders and foils. According to our survey, Y foils [5,19] continue to be largely adopted due to their ease of use, although sputtered Y targets [2,7,18,20] provide superior heat transfer and thus allow higher beam current irradiations. It has also to be kept in mind that the target foils present some handling limitations, especially after irradiation, while sputtered targets suffer from high cost and standardization issues.

To overcome these problems, in this study, the use of the Spark Plasma Sintering (SPS) technique has been investigated for the first time to develop an alternative type of cyclotron solid targets. This new concept has been applied to the production of ^{89}Zr in a medical facility equipped with a solid target station. In this novel approach, a metallic Y disc is placed in contact with a niobium (Nb) backing plate and then tightly bound to it through the SPS technique. Strong adhesion is obtained between the Y foil and the backing plate, thus enhancing the thermal contact between the two metallic sheets. Generally, a performance key parameter for production targets is the ability to effectively remove the heat deposited during irradiation, particularly when high currents are used to increase the production yield [18,21]. Niobium was selected as the backing material due to its high melting temperature (T_m = 2468 °C), sufficient thermal conductivity (53.7 $W{\cdot}m^{-1}{\cdot}K^{-1}$), and high chemical inertness to acidic conditions [22].

This study is dedicated to the manufacturing and experimental testing of a new type of Y target. The aim is to evaluate the potential use of the SPS technique for Y target preparation as a standard routine for medical-grade ^{89}Zr radionuclide production and compare the new method with existing ones.

2. Materials and methods

2.1. Brief description of the SPS technique

In the last decade, the interest toward the Field Assisted Sintering (FAST)/Spark Plasma Sintering (SPS) techniques has been increasing due to its advantages over conventional sintering methods (hot pressing, hot isostatic pressing, high-pressure sintering, etc.). The attractive peculiarities of the SPS technique are the high heating rates (up to 1000 °C/min), fast sintering times (minutes instead of hours), lower sintering temperatures, and the ability to compact hard sintering materials such as nanocrystalline, refractory and metastable materials, starting from powder form [23,24].

Fig. 1 illustrates the general scheme of the SPS process. The powder sample is placed between electrically conductive die and punches, usually made of high-density graphite. The process can be performed in a vacuum or an inert atmosphere. The punches maintain constant uniaxial pressure on the sample, whereas a low-voltage high-intensity electric current is applied through the die and punches, and eventually through the sample itself, generating Joule heating. Simultaneous application of temperature and uniaxial pressure leads to fast densification of metals and ceramics at temperatures consistently lower than traditional methods within just minutes.

In addition to sintering, direct bonding (without binders, adhesive, or welding additives) between different materials is also feasible (e.g., materials having different melting points) [25]. In this work, this latter characteristic has been exploited to achieve an alternative manufacturing technique for supplying a new type of target for cyclotron radionuclide production by bonding commercially available Y metal discs of the desired thickness to a Nb backing plate.

2.2. ^{89}Y target preparation using the SPS technique (YS, YP)

Y discs (99%) of 12 mm diameter and 150 μm thickness (75.8 mg), and Nb discs (99.9%) of 1.0 mm (or 1.7 mm) thickness and 23.5 mm diameter, were purchased from Goodfellow (Cambridge Ltd). Y discs were attached to Nb plates with the SPS technique to produce the final Y targets.

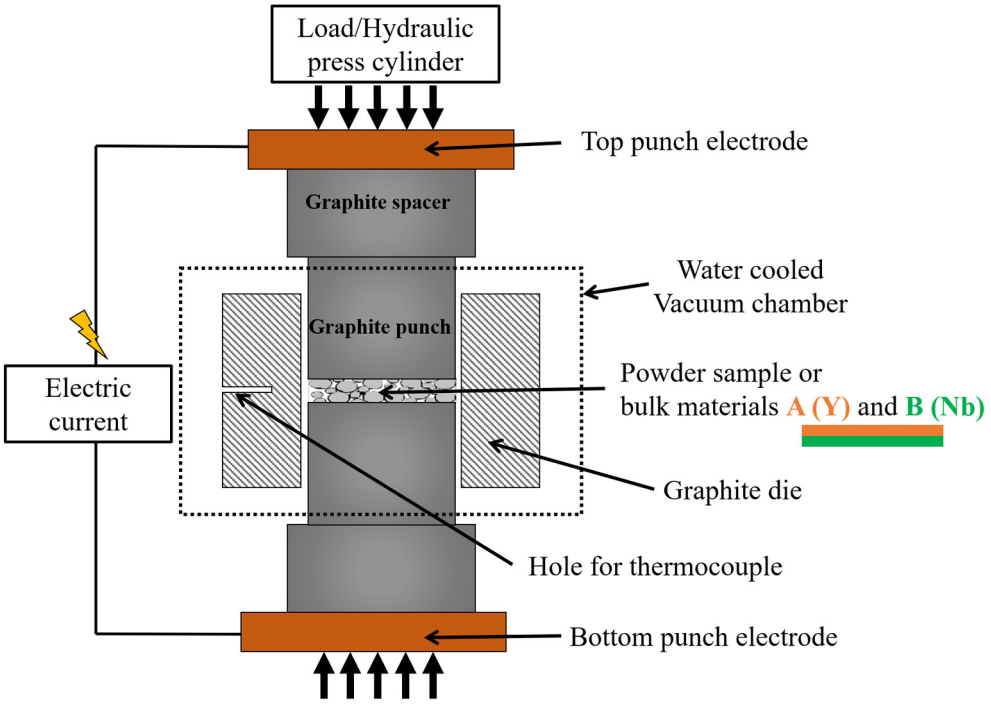

Fig. 1. Spark Plasma Sintering general scheme.

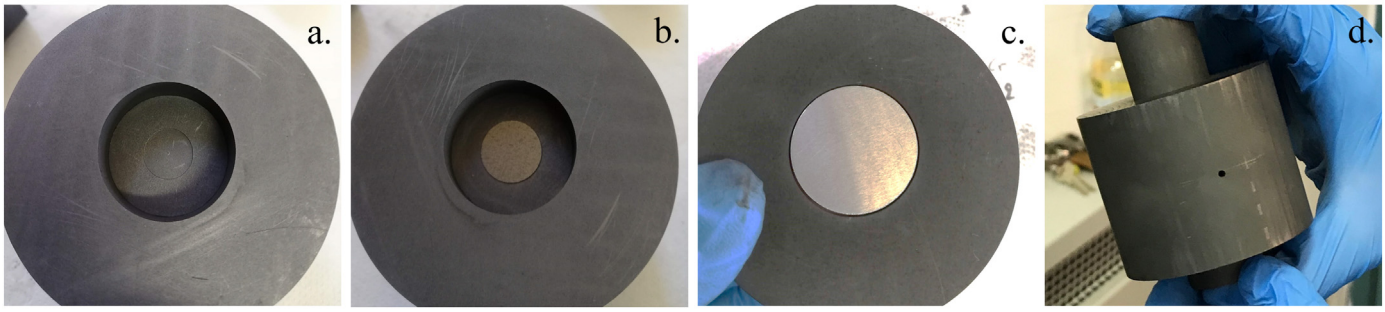

Fig. 2. Assembly of the starting materials, Y foil and Nb disc, in the graphite matrix: a. punch with a central recess; b. Y foil placed in the recess; c. Nb backing disc in the die; d. graphite matrix assembled.

Three Y targets (YS) were manufactured using a Dr. SINTER® model SPS1050 machine (Sumitomo Coal & Mining Ltd., currently SPS Syntex Inc.) applying a current of 1200 A, approximately corresponding to a temperature of 700 °C on the sample.

Three additional Y targets (YP) were manufactured with an INFN prototype machine based on FAST technology, developed at the University of Pavia (Italy) [23,26,27] in the framework of the LARAMED project [28]. The prototype machine presents a simplified layout, AC power supply, off-the-shelf hydraulic, power components, and controllers. Custom-designed high-density graphite dies were used to host the Y disc and the Nb coin during the process, as shown in Fig. 2. The Y disc was inserted into a central recess (diameter = 12.10 mm, depth = 0.1 mm), machined in one of the two graphite punches, to be centered on the Nb coin, which is then inserted into the die with the second punch.

The assembly was then placed inside the processing chamber, as shown in Fig. 3. All experiments were carried out under a vacuum of about 10^{-2} mbar. Uniaxial pressure of 11 MPa on the punch, was exerted through a hydraulic system at the beginning of the experiment (i.e., at room temperature, before starting the heating cycle), maintained throughout the process and removed when turning off the power. The sample was then allowed to cool down. The heating rate was 200 °C/min until the desired temperature of 700 °C was reached, further held for 3 min (Fig. 4). The temperature was measured using a K-type thermocouple (1 mm diameter) inserted into a 10 mm hole drilled in the center of the graphite die wall. Real-time measurements of voltage, current, and temperature have been recorded and stored (Fig. 4).

In this work, the acronym YS stands for Y targets made with the Sumitomo machine, whereas YP refers to Y targets obtained with the INFN prototype machine assembled at the University of Pavia.

2.3. Preparation of the Y foil target (YF)

Y foil targets (YF-1,2) were arranged following the sandwich approach described elsewhere [29]. Briefly, the Y foil (25 mm × 25 mm × 0.15 mm, 99%), purchased from Goodfellow, was cut and glued between a Nb backing, used to ensure an adequate thermal conductivity, and a frontal aluminum (Al) disc (500 μm thickness) to isolate frontal helium cooling. The foil targets were used for comparison with SPS-made targets.

2.4. Cyclotron irradiation

Proton irradiations were carried out with a variable energy (14–19 MeV) TR19 cyclotron (ACSI, Richmond, BC, Canada) equipped with a high-current ion source of up to 300 μA. The solid target station (ACSI) was oriented at 90° and was connected directly to the cyclotron

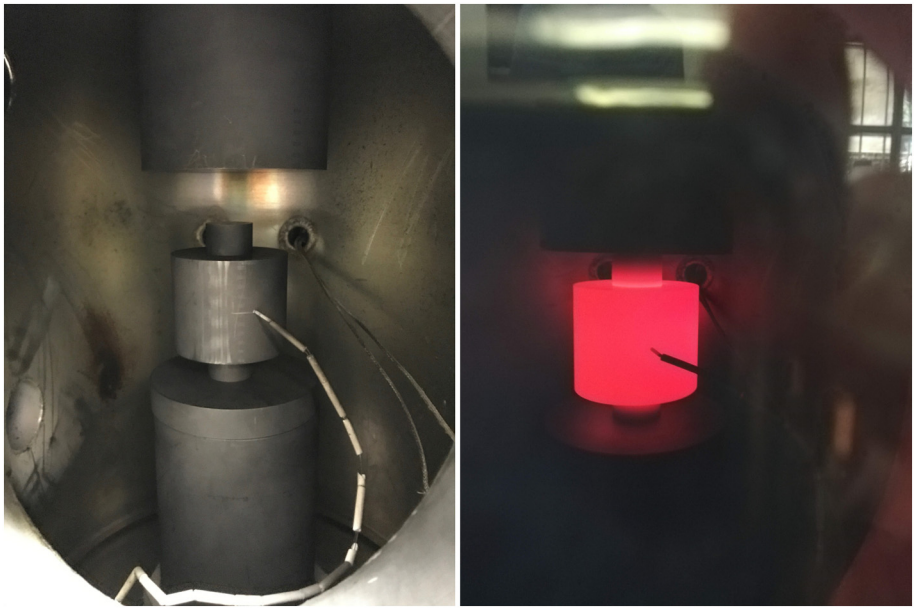

Fig. 3. Image of the system taken through the vacuum chamber window: before applying the loading (left) and during the process (right).

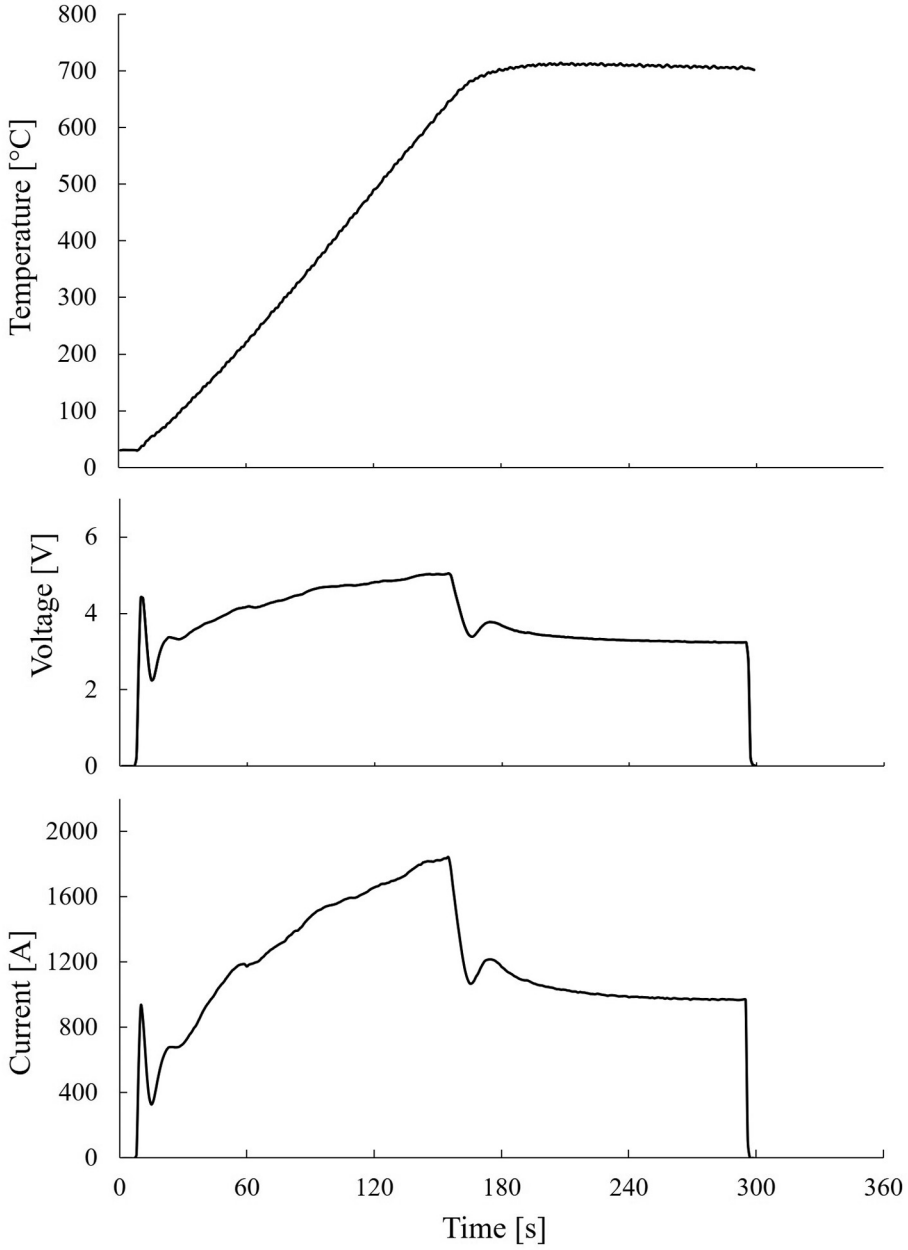

Fig. 4. Trend of the sample temperature, applied voltage and current during the SPS process.

target selector. The target coin was cooled by flushing helium gas onto the front side and water from the backside. The target station was described previously by the authors [18]. The cyclotron target holder could hold a coin with a maximum thickness of 2 mm and a diameter of 24 mm.

The SPS Y target was designed to exactly fit the geometry of the solid target station; whereas, the Y foils were placed between a frontal Al foil and backing Nb disc, in a classical sandwich configuration, to be held on the same target station.

The targets were irradiated for 1 to 5 h with a proton current in the 20–50 μA interval. In all irradiation experiments, the beam size diameter was about 10 mm. Proton energy of 12 MeV on the target material was used. For the Y foils (YF) the starting 16.3 MeV beam was degraded by a 50 μm thick Havar® foil window, used to contain the helium chamber, and a 500 μm thick Al foil, employed for the sandwich configuration assembly. Instead, for the SPS-made targets, the proton beam output energy of 13 MeV was further reduced to 12 MeV once it passed through a 50 μm thick Havar® foil before hitting the Y disc. Calculations were performed with Stopping and Range of Ions in Matter (SRIM) software [30].

After each irradiation, the targets were transferred by a pneumatic transfer system from the cyclotron target station directly to a shielded hot cell for visual inspection to assess their integrity and subsequent processing.

2.5. Separation and purification of ^{89}Zr

Separation and purification were carried out using an automated procedure on a single-use cassette fitted within an Eckert & Ziegler module [31]. The following steps were performed:

1. complete dissolution of the Y material in 2 mL of 2 M HCl in 1 h, at RT;
2. YS and YP targets were entirely submerged in HCl for dissolution, while Y foils were removed from the backing in the case of YF targets.

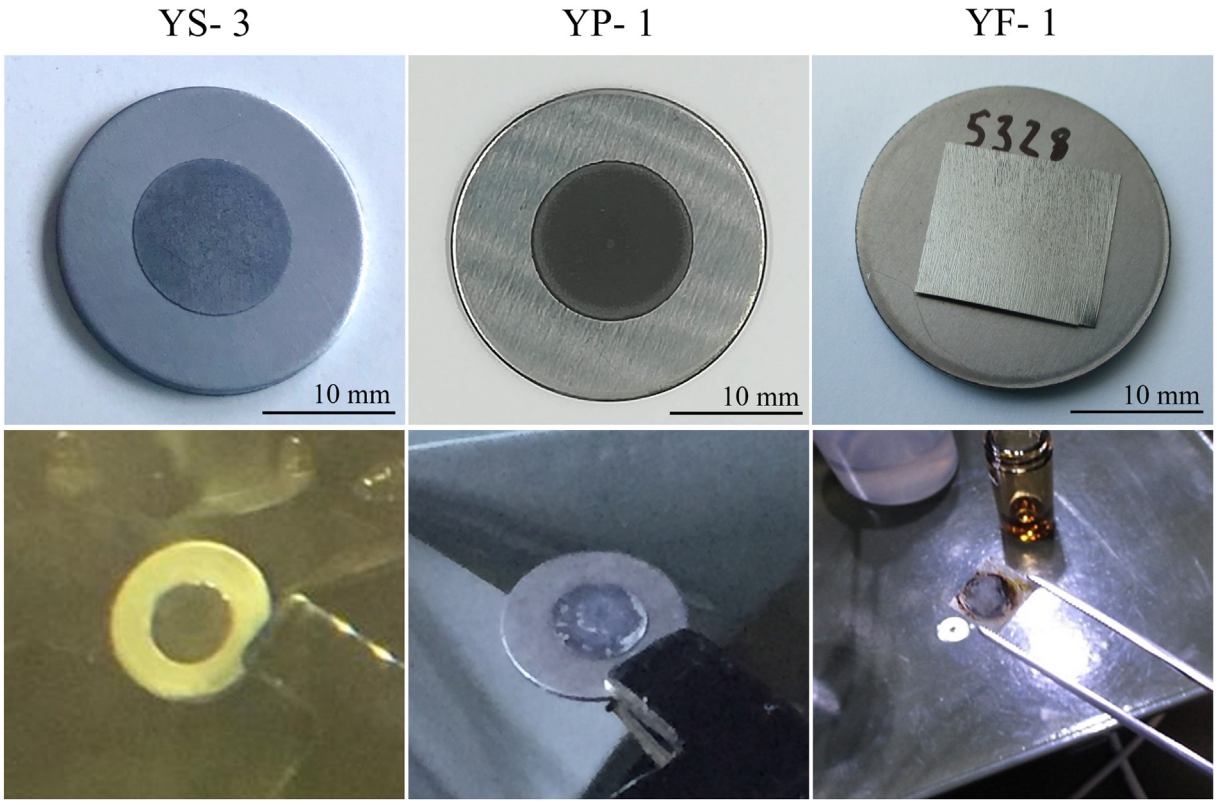

Fig. 5. Y targets before (top) and after (bottom) irradiations.

3. trapping of [^{89}Zr]Zirconium on a ZR-Resin (100 mg of hydroxamate-functionalized resin from Triskem);
4. washing with 20 mL of ultrapure water;
5. recovery of [^{89}Zr]Zirconium from the column with 1.5 mL of 0.5 M aqueous solution of oxalic acid.

Aliquots of the final [^{89}Zr]Zr-oxalate solutions were analyzed by γ-spectroscopy using a high purity germanium gamma detector (HP-Ge, Sw GENIE II Camberra) to determine the amount of [^{89}Zr]Zirconium and radionuclidic impurities.

2.6. Apparent molar activity and radiolabeling

DFO was dissolved in water to obtain a stock solution from which several dilutions were prepared (30-10-3-1-0.3-0.1 μg/mL). Then, 100 μL DFO solution, 150 μL of 0.5 M HEPES (pH = 6.5) and 60–100 μL (21 MBq/0.57 mCi) of the 0.5 M produced [^{89}Zr]Zr-oxalate were mixed with 55 μL of 0.5 M Na_2CO_3 to obtain a final solution with pH = 7.5. After 1 h at RT, resulting solutions of [^{89}Zr]Zr-DFO were analyzed with iTLC-SG 50 mM EDTA (pH = 5) to evaluate the apparent molar activity [10].

Solutions containing the final [^{89}Zr]Zr-oxalate complex were also analyzed by inductively coupled plasma optical emission spectrometry (ICP-OES, Perkin Elmer) to evaluate the presence of different metals such as aluminum, iron, niobium, yttrium and zirconium that could affect the chemical reactivity of ^{89}Zr.

Antibody labeling was performed by reacting [^{89}Zr]Zr-oxalate solutions with DFO-derivatized Trastuzumab [32]. Aliquots (20–600 μL) of [^{89}Zr]Zr-oxalate were added to 50–500 μL of 0.5 M HEPES (pH = 6.5), and finally, the pH was adjusted to 7 by adding 2 M of aqueous Na_2CO_3. The resulting solution was left to stand for 3 min at RT. DFO-Trastuzumab (20–200 μL) was added to the [^{89}Zr]Zr solution, then buffered to pH 7–7.5 by adding 20–200 μL of 0.5 M HEPES (pH = 7.2). The final solution was incubated at 37 °C for 1 h at 550 rpm and then analyzed with iTLC-SG 50 mM EDTA (pH = 5) and with HPLC SEC (Biosep 3000) FM 0.1 M sodium phosphate monobasic, 0.1 M sodium phosphate dibasic and 0.15 M sodium chloride (pH 6.2–7.0) [33].

3. Results

3.1. Cyclotron irradiation

In Fig. 5 a sample of each Y target type (YS, YP, and YF) before and after the irradiations is shown. The irradiation conditions (proton current and energy, irradiation time) are summarized in Table 1.

The entire SPS Y target preparation process took approximately 15 min, and the resulting targets were ready to be inserted into the target station.

A visual inspection after irradiation under the proton beam demonstrated no visible damage to the SPS targets. Each Y target maintained integrity while tested under irradiation conditions, and the Y disc remained firmly attached to Nb.

Table 1
Irradiation conditions and ^{89}Zr saturation yields. All activities have been decay-corrected to the end-of-bombardment time for each production run.

Target	Current [μA]	Energy on target [MeV]	Time [min]	Saturation yield [MBq/μAh] (mCi/μAh)
YS-1	36.2	12.0	264	13.876 (0.375)
YS-2	48.6	12.0	302	14.699 (0.397)
YS-3	49.6	12.0	158	13.719 (0.371)
YP-1	48.6	12.0	158	14.190 (0.384)
YP-2	46.8	12.0	62	13.861 (0.375)
YP-3	49.7	12.0	190	14.404 (0.389)
YF-1	46.3	12.0	61	14.236 (0.385)
YF-2	47.0	12.0	60	14.430 (0.390)

Table 2
Activity measured in the recovery process for the irradiated targets.

Target	Activity in bulk solution [MBq] (mCi)	Waste activity [MBq] (mCi)	Zr SPE Activity [MBq] (mCi)	[^{89}Zr]Ox collected [MBq] (mCi)	^{89}Zr recovery %
YS-1	2569.28 (69.44)	333 (9)	27.75 (0.75)	2208.53 (59.69)	86.0
YS-2	3947.53 (106.69)	310.06 (8.38)	42.55 (1.15)	3579.92 (97.16)	91.1
YS-3	1916.97 (51.81)	122.1 (3.30)	4.07 (0.11)	1794.5 (48.5)	93.6
YP-1	1905.13 (51.49)	66.97 (1.81)	22.2 (0.6)	1816.7 (49,1)	95.3
YP-2	704.85 (19.05)	22.2 (0.6)	12.95 (0.35)	669.7 (18.1)	95.0
YP-3	2332.85 (63.05)	52.54 (1.42)	12.95 (0.35)	2267.36 (61.28)	97.2
YF-1	702.26 (18.98)	25.9 (0.70)	3.7 (0.10)	672.66 (18.18)	95.8
YF-2	703.74 (19.02)	20.72 (0.56)	7.4 (0.20)	675.62 (18.26)	96.0

The YF targets were arranged on the Nb disc before irradiation, and the Y foils were removed manually with a tweezer after the proton bombardment. Some damage signs were visible on the aluminum foil after irradiation at 50 μA.

3.2. Separation and purification

Tables 1 and 2 summarize the irradiation conditions, the ^{89}Zr saturation yield, and the recovery evaluation for each target.

The average saturation yield of ^{89}Zr produced using the SPS targets was 14.12 ± 0.38 MBq/μAh ($n = 6$). After purification, 93 ± 4% (n = 6) of loaded ^{89}Zr was recovered in 1.5 mL of 0.5 M oxalic acid solution. Similar saturation yield and recovery values were obtained using Y foils, 14.33 ± 0.14 MBq/μAh and 96 ± 0.14% ($n = 2$), respectively.

In Table 2, the detailed activities of the bulk solution, waste, Zr SPE, and [^{89}Zr]Zr-oxalate, corrected for the end-of-bombardment (EOB) time for each production, are reported.

The recovery procedures were performed for all irradiated targets, and all components were measured to evaluate the process. The average recovery percentage was 93 ± 4%. High recovery values were obtained by slowing the loading onto the Zr cartridge and keeping the oxalate solution on SPE for 1 min before elution.

3.3. Molar activity, impurity evaluation, and radiolabeling

Gamma-spectroscopy was performed on all [^{89}Zr]Zr-oxalate solutions immediately after recovery, and 1 month, 3 months, and 6 months after the EOB, to evaluate the possible presence of long-lived impurities. Only two peaks with high intensity at 511 and 909 keV, both corresponding to ^{89}Zr radionuclide, were detected after each acquisition time. Fig. 6 shows a representative γ-spectrum acquired one day after the EOB.

Table 3 summarizes the values related to the metal content analyzed by ICP-OES carried out on YS-3, YP-1, and YF-1 samples.

ICP-OES analysis was performed to measure the concentration of other impurities present in the final solution that could affect [^{89}Zr]Zr-oxalate reactivity and allow the correct purification and backing resistance assessments.

The evaluation of chemical purity was carried out with iTLC-SG 50 mM EDTA (pH = 5), and the molar activity (A_m) was calculated by DFO titration, resulting in 140 ± 28.3 GBq/μmol for YS, 143.3 ± 59.4 GBq/μmol for YP, and 46 ± 5.6 GBq/μmol for YF. Table 4 reports detailed results on the activity collected after purification.

[^{89}Zr]Zr-DFO-Trastuzumab was successfully labeled with high yield (99%–100% by HPLC, see Fig. 7, and TLC) with ^{89}Zr produced from all targets and with specific activity (A_s) as reported in Table 5.

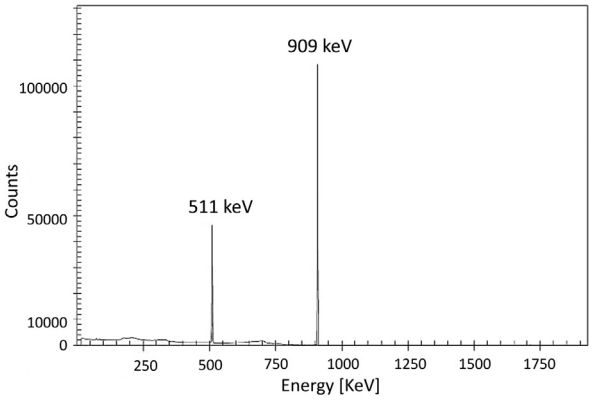

Fig. 6. Representative γ-spectrum of [^{89}Zr]Zr-Oxalate acquired one day after the EOB.

4. Discussion

The growing interest of ^{89}Zr in nuclear medicine has been demonstrated in several studies [34,35], as also emphasized by an ongoing coordinated research project organized by the International Atomic Energy Agency (IAEA CRP) [6]. To date, ^{89}Y(p,n)^{89}Zr has been considered the optimal nuclear reaction route for the production of ^{89}Zr in medical cyclotrons due to the easy availability of the target material in natural form. However, an open issue is related to the most efficient type of target that may allow achieving the highest yield with minimal production of related impurities [3]. Previous works have already focused on different techniques that lead to the fabrication of all types of targets in the form of foils, pellets, sputtered, electrodeposited layers, and solutions [15,36].

In this work, the SPS technique was used, for the first time, to produce solid Y targets, where Y discs were made to tightly adhere to Nb backing plates without the need for additional binder materials. The affordable already available Y discs were used as the target material form, instead of the Y powder, for two main reasons: (i) the Y powder is highly flammable and thus a controlled atmosphere is required for its handling; (ii) to avoid the further step of Y pellet realization before the bonding to Nb backing.

Three targets were prepared using a commercial machine (YS-1, 2, 3) and three targets using a prototype one (YP-1, 2, 3). Irradiation tests at 12 MeV with a maximum current of 50 μA, corresponding to a power deposition per unit area of approximately 650 W/cm^2, were reported to make a comparison between the yield and quality of the ^{89}Zr radionuclide produced using the two types of targets (YS and YP, both compared to YF).

The results presented here demonstrate that SPS-made Y targets constitute an innovative and feasible alternative approach for the production of ^{89}Zr, comparable to that based on the use of Y foil in terms of ^{89}Zr saturation yield, recovery, and purity. One of the main advan-

Table 3
ICP-OES analysis of [^{89}Zr]Zr-Oxalate solutions for each target type. The error related to the ICP-OES calibration methods is reported.

Target	Y-89 (ppb)	Zr-90 (ppb)	Nb-93 (ppb)	Al-27 (ppb)	Fe-56 (ppb)
YS-3	989 ± 6	<LOD	73.8 ± 6.6	7110 ± 54	581 ± 86
YP-1	172 ± 5	<LOD	<LOD	468 ± 34	323 ± 54
YF-1	1020 ± 8	<LOD	<LOD	53,004 ± 305	242 ± 12

Table 4
Average molar activity and recovered activity from all [^{89}Zr]Zr-Oxalate solutions.

Sample	A_m [GBq/μmol]	ZrOx recovered activity [MBq]	ZrOx recovered activity [mCi]
YS ($n = 3$)	140 ± 28.3	2527 ± 968	68.3 ± 26.2
YP (n = 3)	143.3 ± 59.4	1584 ± 811	42.8 ± 21.9
YF (n = 2)	46 ± 5.6	674 ± 2	18.2 ± 0.1

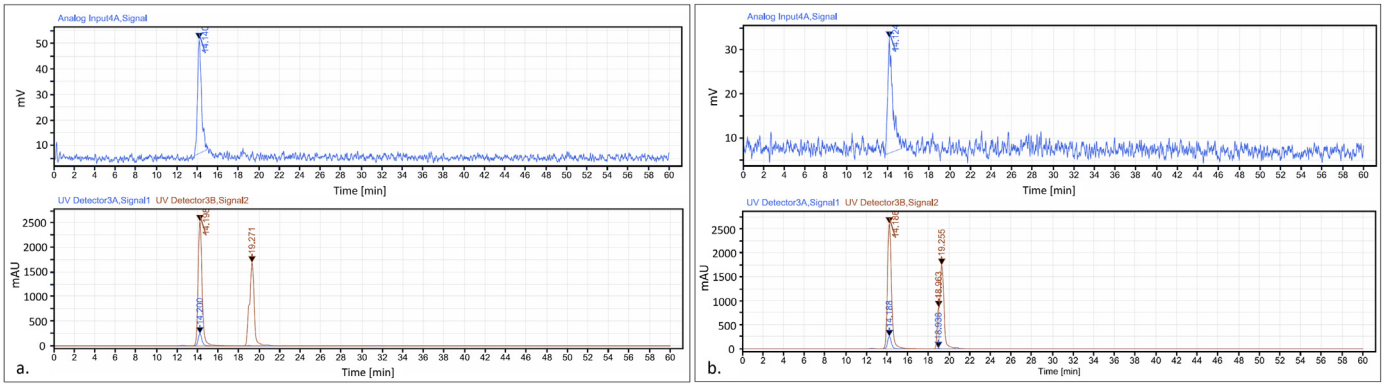

Fig. 7. HPLC SEC [^{89}Zr]Zr-DFO-Trastuzumab: a. 20 h and b. 72 h.

tages is the possibility of processing and handling the SPS targets more easily if compared to standard targets commonly used in previous studies. As shown in Fig. 5, the SPS Y targets allow easy handling by a telemanipulator inside a conventional hot cell, reducing the radiation exposure of the operator. They can be directly entirely loaded into the dissolution module without the need of disassembling it before dissolution, and they still maintain high levels of inertness while minimizing metal contamination. In contrast, the Y foils have to be disassembled manually with tweezers.

The target processing was carried out in 1 h, at RT with 2 mL of 2 M HCl, and allowed complete dissolution of the Y discs and foils. As shown in Tables 2 and 3, no significant differences were found, in terms of saturation yield, between the types of targets (14.12 ± 0.38 MBq/μAh for SPS targets and 14.33 ± 0.14 MBq/μAh for YF) and similar recovery efficiency (93 ± 4% for SPS targets and 96 ± 0.14% for YF) of total activity was achieved. Molar activities of 143.3 ± 59.4 GBq/μmol and 140 ± 28.3 GBq/μmol were calculated for SPS targets manufactured with the SPS prototype machine (YP) and the commercial one (YS), respectively. These results are consistent with the values previously reported [8], whereas foil experiments showed a lower value. DFO-Trastuzumab labeling was carried out with purified [^{89}Zr]Zr-oxalate solution (130–325 MBq/mL) and the labeling yields resulted in the 99%–100% interval. The radiochemical purity of [^{89}Zr]Zr-DFO-Trastuzumab was evaluated at different time points and the conjugate remained stable up to 72 h after the EOB. The γ-spectroscopy spectrum showed peaks only at 511 and 909 keV, which are the characteristic γ-emissions from ^{89}Zr, resulting in an overall radionuclidic purity of 99.99%, as illustrated in Fig. 6. Acquisitions after 3 and 6 months post EOB confirmed the absence of long-lived radioisotope contaminations.

The presence of some metal impurities revealed by the ICP-OES analysis, shown in Table 3, is probably due to the Nb backing disc because the entire SPS-made targets (Y—Nb) were placed in contact with the HCl solution to dissolve the Y disc. Even though Nb is meant to be chemically resistant to HCl, some impurities could be released in the solution, anyway. In planned future experiments, a dedicated dissolution reactor system based on an open-bottomed vial that confines the solution only to a small surface area of the backing disc [37,38] will be used to reduce such impurities. However, the high metallic Y residue needs to be investigated in further dissolution tests.

Besides, the ICP-OES analysis on the foil samples showed a high aluminum concentration, likely originating from the Al foil placed in contact with the Y foil, used as a container and beam energy degrader. Indeed, after the irradiation at 50 μA, some damage signs were visible on the aluminum foil so, traces of material could be transferred to the Y foil. On the contrary, all SPS-made targets preserved their integrity after irradiation under the described conditions. Even after the irradiation test at 60 μA, no sign of damage was detected by visual inspection on the targets made with SPS (results not yet published). However, in this work, 50 μA was chosen as the maximum current value to compare the ^{89}Zr radionuclide yield produced using Y foil and SPS-made targets.

From a thermomechanical point of view, the Y—Nb tight bonding, obtained by SPS, might cause to reduce the thermal resistance between contact materials, thus to more efficient heat exchange with the water-cooling system. Moreover, the SPS-made targets do not need Al foil. In this way, the He flow is in direct contact with the Y disc bonded to the Nb backing, enhancing the cooling efficiency. The resulting more efficient thermal power exchange between the SPS-made target and the cooling system, occurring during the irradiation phase, paves the way for the use of the SPS technique to manufacture more robust solid targets capable of withstanding higher proton current irradiations, which could be employed to obtain larger radionuclide yield.

Similarly, the sputtered targets, which have been investigated by Queern et al. [7] and the authors [18], could present the same advantages. However, the SPS technique presents the following benefits: (i) faster process, (ii) no Y material losses during the manufacturing, (iii) thickness uniformity, and (iv) the possibility of using thicker discs to increase and optimize the ^{89}Zr production.

Further studies are ongoing to understand better the nature of the metallurgical Y—Nb interface that is achieved during the SPS process, which certainly affects the total thermal conductivity. Moreover, it is necessary to investigate how increased thickness and purity (> 99%)

Table 5
Average specific activity for [^{89}Zr]Zr-DFO-Trastuzumab.

Sample	A_s [MBq/mg]
YS	20.9
YP	26.7
YF	12.6

of Y, a dedicated designed reactor for the dissolution and separation process to ensure safer handling procedures and higher proton currents, influence the production yield of ^{89}Zr.

Overall, the results described in this work provide a significant first step toward using the SPS technique for alternative efficient manufacturing of solid cyclotron targets for medical radioisotope production. It is important to emphasize that SPS is a rapid and easily manageable technology that allows to sintering high-quality objects with desired density and thickness, starting from different materials in powder form. Because substantial losses of starting materials are almost negligible, this technique seems extremely attractive for producing targets composed of quite expensive isotopically enriched materials, provided in metallic or oxide powder form. Therefore, the SPS technique might be a feasible alternative to realize solid targets for other emerging radioisotopes [28,39].

5. Conclusions

In the present research work, the feasibility study on the SPS technique for cyclotron solid targets manufacturing aimed at radionuclide production has been carried out. In particular, its advantages were exploited here to manufacture Y targets for ^{89}Zr production. The results showed that the SPS technique allows a tight bonding of Y metal disc to a Nb disc, thus resulting in a robust target suitable to tolerate high on-target currents without degradation. One of the more significant findings emerging from this study is that the SPS-made targets are easily handled for further purification steps post-irradiation. After the dissolution and purification processes, the production yields and the radioimpurity profile of the final ^{89}Zr were comparable to the results obtained with foil targets. Finally, the reactivity of [^{89}Zr]Zr-oxalate, prepared using ^{89}Zr -produced by SPS, was evaluated by reaction with DFO to assess A_m and by labeling the DFO-Trastuzumab conjugated antibody following previously reported procedures. The results were well consistent with literature data, thus showing that the quality of ^{89}Zr produced by the SPS-made target is adequate to perform labeling studies to develop new radiopharmaceuticals based on ^{89}Zr.

Acknowledgments

The authors would like to thank Dr. Gaia Pupillo, Dr. L. Mou, and G. Sciacca for helpful discussions. The work was performed in the framework of the LARAMED (LAboratory of RAdioisotopes for MEDicine) research program (funded by Ministry of Education, University and Research, MUR, Italy), running at Istituto Nazionale di Fisica Nucleare - Laboratori Nazionali di Legnaro (INFN-LNL), Italy.

References

[1] van de Watering FCJ, Rijpkema M, Perk L, Brinkmann U, Oyen WJG, Boerman OC. Zirconium-89 labeled antibodies: a new tool for molecular imaging in cancer patients. Biomed Res Int. 2014;2014:1–13. https://doi.org/10.1155/2014/203601.
[2] Verel I, Visser GWM, Boellaard R, Walsum MS, Snow GB, van Dongen GAMS. 89Zr immuno-PET: comprehensive procedures for the production of 89Zr-labeled monoclonal antibodies. J Nucl Med. 2003;44:1271–81.
[3] Jalilian AR, Osso JA. Production, applications and status of zirconium-89 immunoPET agents. J Radioanal Nucl Chem. 2017;314:7–21. https://doi.org/10.1007/s10967-017-5358-z.
[4] Sharifian M, Sadeghi M, Alirezapour B, Yarmohammadi M, Ardaneh K. Modeling and experimental data of zirconium-89 production yield. Appl Radiat Isot. 2017;130:206–10. https://doi.org/10.1016/j.apradiso.2017.09.044.
[5] Wooten A, Madrid E, Schweitzer G, Lawrence L, Mebrahtu E, Lewis B, et al. Routine production of 89Zr using an automated module. Appl Sci. 2013;3:593–613. https://doi.org/10.3390/app3030593.
[6] Production of Zirconium-89 and the development of Zr-89 radiopharmaceuticals. https://www.iaea.org/projects/crp/f22071; 2017. (accessed April 1, 2020).
[7] Queern SL, Aweda TA, Massicano AVF, Clanton NA, El Sayed R, Sader JA, et al. Production of zr-89 using sputtered yttrium coin targets. Nucl Med Biol. 2017;50:11–6. https://doi.org/10.1016/j.nucmedbio.2017.03.004.
[8] Alnahwi A, Tremblay S, Guérin B. Comparative study with 89Y-foil and 89Y-pressed targets for the production of 89Zr †. Appl Sci. 2018;8:1579. https://doi.org/10.3390/app8091579.
[9] Dias GM, Ramogida CF, Rousseau J, Zacchia NA, Hoehr C, Schaffer P, et al. 89 zr for antibody labeling and in vivo studies – a comparison between liquid and solid target production. Nucl Med Biol. 2018;58:1–7. https://doi.org/10.1016/j.nucmedbio.2017.11.005.
[10] Holland JP, Sheh Y, Lewis JS. Standardized methods for the production of high specific-activity zirconium-89. Nucl Med Biol. 2009;36:729–39. https://doi.org/10.1016/j.nucmedbio.2009.05.007.
[11] Infantino A, Cicoria G, Pancaldi D, Ciarmatori A, Boschi S, Fanti S, et al. Prediction of 89Zr production using the Monte Carlo code FLUKA. Appl Radiat Isot. 2011;69:1134–7. https://doi.org/10.1016/j.apradiso.2010.11.027.
[12] Bhatt N, Pandya D, Wadas T. Recent advances in Zirconium-89 chelator development. Molecules. 2018;23:638. https://doi.org/10.3390/molecules23030638.
[13] George KJH, Borjian S, Cross MC, Hicks JW, Schaffer P, Kovacs MS. Expanding the PET radioisotope universe utilizing solid targets on small medical cyclotrons. RSC Adv. 2021;11:31098–123. https://doi.org/10.1039/D1RA04480J.
[14] Pandey MK, DeGrado TR. Cyclotron production of PET radiometals in liquid targets: aspects and prospects. CRP. 2020;13. https://doi.org/10.2174/1874471013999200820165734.
[15] Pandey MK, Engelbrecht HP, Byrne JF, Packard AB, DeGrado TR. Production of 89Zr via the 89Y(p, n)89Zr reaction in aqueous solution: effect of solution composition on in-target chemistry. Nucl Med Biol. 2014;41:309–16. https://doi.org/10.1016/j.nucmedbio.2014.01.006.
[16] Zacchia NA, Martinez DM, Hoehr C. Radiolysis reduction in liquid solution targets for the production of 89Zr. Appl Radiat Isot. 2020;155:108791. https://doi.org/10.1016/j.apradiso.2019.06.037.
[17] Pandey MK, Bansal A, Engelbrecht HP, Byrne JF, Packard AB, DeGrado TR. Improved production and processing of 89Zr using a solution target. Nucl Med Biol. 2016;43:97–100. https://doi.org/10.1016/j.nucmedbio.2015.09.007.
[18] Skliarova H, Cisternino S, Cicoria G, Marengo M, Cazzola E, Gorgoni G, et al. Medical cyclotron solid target preparation by ultrathick film magnetron sputtering deposition. Instruments. 2019;3:21. https://doi.org/10.3390/instruments3010021.
[19] Link JM, Krohn KA, O'Hara MJ. A simple thick target for production of 89 zr using an 11 MeV cyclotron. Appl Radiat Isot. 2017;122:211–4. https://doi.org/10.1016/j.apradiso.2017.01.037.
[20] Meijs WE, Herscheid JDM, Haisma HJ, Wijbrandts R, van Langevelde F, Van Leuffen PJ, et al. Production of highly pure no-carrier added 89Zr for the labelling of antibodies with a positron emitter. Appl Radiat Isot. 1994;45:1143–7. https://doi.org/10.1016/0969-8043(94)90029-9.
[21] Skliarova H, Cisternino S, Cicoria G, Marengo M, Palmieri V. Innovative target for production of technetium-99m by biomedical cyclotron. Molecules. 2018;24:25. https://doi.org/10.3390/molecules24010025.
[22] Asselin E, Ahmed TM, Alfantazi A. Corrosion of niobium in sulphuric and hydrochloric acid solutions at 75 and 95°C. Corros Sci. 2007;49:694–710. https://doi.org/10.1016/j.corsci.2006.05.028.
[23] Anselmi-Tamburini U, Groza JR. Critical assessment 28: electrical field/current application – a revolution in materials processing/sintering? Mater Sci Technol. 2017;33:1855–62. https://doi.org/10.1080/02670836.2017.1341692.
[24] Cavaliere P. Spark plasma sintering of materials: advances in processing and applications. Cham: Springer International Publishing; 2019. https://doi.org/10.1007/978-3-030-05327-7.
[25] Hu Z-Y, Zhang Z-H, Cheng X-W, Wang F-C, Zhang Y-F, Li S-L. A review of multi-physical fields induced phenomena and effects in spark plasma sintering: fundamentals and applications. Materials & Design. 2020;191:108662. https://doi.org/10.1016/j.matdes.2020.108662.
[26] Chen W, Anselmi-Tamburini U, Garay JE, Groza JR, Munir ZA. Fundamental investigations on the spark plasma sintering/synthesis process. Mater Sci Eng A. 2005;394:132–8. https://doi.org/10.1016/j.msea.2004.11.020.
[27] Anselmi-Tamburini U, Gennari S, Garay JE, Munir ZA. Fundamental investigations on the spark plasma sintering/synthesis process. Mater Sci Eng A. 2005;394:139–48. https://doi.org/10.1016/j.msea.2004.11.019.
[28] Esposito J, Bettoni D, Boschi A, Calderolla M, Cisternino S, Fiorentini G, et al. LARAMED: a laboratory for radioisotopes of medical interest. Molecules. 2019;24:20. https://doi.org/10.3390/molecules24010020.
[29] Ciarmatori A, Cicoria G, Pancaldi D, Infantino A, Boschi S, Fanti S, et al. Some experimental studies on 89 zr production. Radiochim Acta. 2011;99:631–4. https://doi.org/10.1524/ract.2011.1822.
[30] James Ziegler - SRIM & TRIM n.d. http://www.srim.org/.
[31] Lin M, Mukhopadhyay U, Waligorski GJ, Balatoni JA, González-Lepera C. Semi-automated production of 89Zr-oxalate/89Zr-chloride and the potential of 89Zr-chloride in radiopharmaceutical compounding. Appl Radiat Isot. 2016;107:317–22. https://doi.org/10.1016/j.apradiso.2015.11.016.
[32] Vosjan MJWD, Perk LR, Visser GWM, Budde M, Jurek P, Kiefer GE, et al. Conjugation and radiolabeling of monoclonal antibodies with zirconium-89 for PET imaging using the bifunctional chelate p-isothiocyanatobenzyl-desferrioxamine. Nat Protoc. 2010;5:739–43. https://doi.org/10.1038/nprot.2010.13.
[33] Dias GM, Ramogida CF, Rousseau J, Zacchia NA, Hoehr C, Schaffer P, et al. 89 zr for antibody labeling and in vivo studies – a comparison between liquid and solid target production. Nucl Med Biol. 2018;58:1–7. https://doi.org/10.1016/j.nucmedbio.2017.11.005.
[34] Telix International Pty Ltd. A confirmatory, prospective, open-label, multi-centre phase 3 study to evaluate diagnostic performance of zirconium-labelled girentuximab to non-invasively detect ccRCC by PET/CT imaging in patients with indeterminate renal masses. clinicaltrials.gov; 2021.
[35] Merkx RIJ, Lobeek D, Konijnenberg M, Jiménez-Franco LD, Kluge A, Oosterwijk E, et al. Phase I study to assess safety, biodistribution and radiation dosimetry for 89Zr-girentuximab in patients with renal cell carcinoma. Eur J Nucl Med Mol Imaging. 2021. https://doi.org/10.1007/s00259-021-05271-w.

[36] Kasbollah A, Eu P, Cowell S, Deb P. Review on production of 89Zr in a medical cyclotron for PET radiopharmaceuticals. J Nucl Med Technol. 2013;41:35–41. https://doi.org/10.2967/jnmt.112.111377.
[37] Palmieri V, Skliarova H, Cisternino S, Marengo M, Cicoria G. Method for obtaining a solid target for radiopharmaceuticals production; 2019 Patent no. WO/2019/053570.
[38] Sciacca G, Martini P, Cisternino S, Mou L, Amico J, Esposito J, et al. A universal cassette-based system for the dissolution of solid targets. Molecules. 2021;26:6255. https://doi.org/10.3390/molecules26206255.
[39] Skliarova H, Cisternino S, Cicoria G, Cazzola E, Gorgoni G, Marengo M, et al. Cyclotron solid targets preparation for medical radionuclides production in the framework of LARAMED project. J Phys Conf Ser. 2020;1548:012022. https://doi.org/10.1088/1742-6596/1548/1/012022.